minerals

MDPI

Article

Regional-Scale Paleoproterozoic Heating Event on Archean Acasta Gneisses in Slave Province, Canada: Insights from K–Ar and ^{40}Ar/^{39}Ar Chronology

Megumi Sato [1,†], Hironobu Hyodo [1,2], Kei Sugiura [3], Tatsuki Tsujimori [3,4] and Tetsumaru Itaya [5,6,7,*]

1 Graduate School of Science, Okayama University of Science, Okayama 700-0005, Japan; dian-0818@ka.tnc.ne.jp (M.S.); hhyodo@gmail.com (H.H.)
2 Institute of Frontier Science and Technology, Okayama University of Science, Okayama 700-0005, Japan
3 Department of Earth Science, Graduate School of Science, Tohoku University, Aoba, Sendai 980-8578, Japan; sugiura.kei.q8@dc.tohoku.ac.jp (K.S.); tatsukix@tohoku.ac.jp (T.T.)
4 Center for Northeast Asian Studies, Tohoku University, Aoba, Sendai 980-8576, Japan
5 Hiruzen Institute for Geology & Chronology, 2-5 Nakashima, Naka-ku, Okayama 703-8252, Japan
6 Japan Geochronology Network, 2-12 Nakashima, Naka-ku, Okayama 703-8252, Japan
7 Institute of GeoHistory, Japan Geochronology Network, 1599 Susai, Akaiwa 701-2503, Japan
* Correspondence: tetsumaru.itaya@gmail.com
† Current address: Nameri 500-2-103, Nagaizumi, Suntō District, Shizuoka 411-0933, Japan.

Abstract: Slave Province in Canada is an Archean granite–supracrustal terrane at the northwestern corner of the Canadian Shield. It is bordered by the Thelon–Taltson orogen (2.0 to 1.9 Ga) to the southeast and the Wopmay orogen (1.9 to 1.8 Ga) to the west. Acasta gneisses, exposed in the westernmost Slave Province, and the Wopmay rocks, located close to the gneisses, were systematically collected for K–Ar and laser step-heating ^{40}Ar/^{39}Ar single-crystal analyses of the biotite and amphibole. The K–Ar biotite ages of the four Wopmay samples range from 1816 ± 18 Ma to 1854 ± 26 Ma. The ^{40}Ar/^{39}Ar biotite analyses of the three Wopmay samples yield plateau ages of 1826 ± 21 Ma, 1886 ± 13 Ma, and 1870 ± 18 Ma. These ages fall within the reported U–Pb zircon age range of the Wopmay orogen. The K–Ar biotite ages of the fifteen Acasta gneisses range from 1779 ± 25 Ma to 1877 ± 26 Ma, except for one younger sample (1711 ± 25 Ma). The ^{40}Ar/^{39}Ar analyses of the biotite crystals from three samples give the plateau ages of 1877 ± 8 Ma, 1935 ± 14 Ma, and 1951 ± 11 Ma. The K–Ar amphibole ages from twelve samples range from 1949 ± 19 Ma to 1685 ± 25 Ma. Two samples of them give ages older than the zircon U-Pb age of Hepburn plutons. The ^{40}Ar/^{39}Ar analyses of the amphibole crystals show varied age relations. The two samples give plateau ages of 1814 ± 22 Ma and 1964 ± 12 Ma. Some samples exhibit apparent old ages of ~2000 Ma in the middle temperature fractions. These old fractions result from the amphibole crystals, originally formed in the Archean, being affected by the thermal events during the Wopmay orogeny but not fully resetting. These observations suggest that the K–Ar system ages of the biotite and amphibole in the Archean Acasta gneiss were rejuvenated during the Paleoproterozoic ages. The Discussion explores the possibility that the heat source rejuvenating the K–Ar system ages may have arisen due to asthenospheric extrusion into the wedge mantle, a process likely triggered by subduction rollback.

Keywords: K–Ar age; ^{40}Ar/^{39}Ar age; biotite; amphibole; Acasta gneiss; Wopmay orogen; Canada

Citation: Sato, M.; Hyodo, H.; Sugiura, K.; Tsujimori, T.; Itaya, T. Regional-Scale Paleoproterozoic Heating Event on Archean Acasta Gneisses in Slave Province, Canada: Insights from K–Ar and ^{40}Ar/^{39}Ar Chronology. *Minerals* **2024**, *14*, 397. https://doi.org/10.3390/min14040397

Academic Editor: Jim Lee

Received: 22 December 2023
Revised: 3 April 2024
Accepted: 5 April 2024
Published: 12 April 2024

1. Introduction

Slave Province is a well-exposed Archean terrane located in the northwestern corner of the Canadian Shield. It is bordered by the Thelon–Taltson orogen (2.0 to 1.9 Ga) to the southeast and the Wopmay orogen (1.9 to 1.8 Ga) to the west [1,2]. The Acasta gneisses are exposed along the Acasta river in the westernmost Slave Province (Figure 1) [1,3]. Bowring et al. [3] carried out a SHRIMP U–Pb analysis of zircon from the Acasta gneiss and identified the source rock of the Acasta gneiss in the Slave Province as the oldest (3.96 Ga) supracrustal rock on Earth at that time. Iizuka et al. [4] reported 4.20 ± 0.06 Ga zircon xenocryst in an Acasta gneiss and argued for early continental crust. Iizuka et al. [5] created a geological map of the main area of the Acasta gneiss (around the sample locality of the Acasta gneisses reported by Bowring et al. [3]) and sketch maps of critical outcrops and carried out U–Pb analyses of zircon. They revealed at least four tectonothermal events, based on detailed field observations and zircon U–Pb geochronology. Guitreau et al. [6] summarized the geological events that occurred at the Acasta Gneiss Complex, showing the crystallization of the zircon core (4.2 Ga), the formation of the oldest diorites and tonalities, the tonalite formation, the granodiorite formation and the associated anatexis, the regional metamorphism with granitoid formation, and the granite intrusion (2.6 Ga), all based on zircon U–Pb geochronology. They also proposed the Wopmay orogen event using the $^{40}Ar/^{39}Ar$ ages of biotite and amphibole in the Acasta gneiss reported by Hodges et al. [7], because the $^{40}Ar/^{39}Ar$ ages were within the zircon U–Pb ages of the Wopmay orogen. This may mean that the K–Ar system ages of biotite and amphibole in the Acasta gneiss were rejuvenated when the Wopmay orogeny took place in the Paleoproterozoic period. The purpose of this paper is to elucidate how the Wopmay orogeny affected the argon isotope systematics of the Acasta gneiss.

We report the K–Ar and $^{40}Ar/^{39}Ar$ ages of biotite and amphibole from the Acasta gneisses, collected systematically along a traverse 18 km east–west stretch. Based on the age results, we outline the argon isotope systematics of the Archean Acasta gneiss that was affected by the Paleoproterozoic Wopmay orogeny and discuss the heat source that rejuvenated the K–Ar system ages.

2. Geological Setting

The Slave Province is an Archean granite–supracrustal terrane located at the northwestern corner of the Canadian Shield; it covers an area of approximately 190,000 km^2 [1]. It is bounded to the southeast by the Thelon–Taltson orogen (2.0 to 1.9 Ga) and to the west by the Wopmay orogen (1.9 to 1.8 Ga) [1,2] (Figure 1A). It consists mainly of the Yellowknife Supergroup, which is composed of metasedimentary and metavolcanic rocks (2.72 to 2.65 Ga) that are exposed throughout the province [8] and plutons (2.62 to 2.58 Ga) that are seen throughout the entire province [9]. The metavolcanic rock area is called the Greenstone Zone and consists of basic volcanic and plutonic rocks. The basement gneisses older than the Yellowknife are distributed in the western part of the Slave Province. The Acasta gneiss Complex studied in this paper is exposed along the Acasta River in the westernmost part of the Slave Province (Figure 1A). The complex has a heterogeneous assemblage of biotite–amphibole tonalitic-to-granitic orthogneiss. Large areas of amphibolite also occur, together with less abundant calc–silicate gneiss, quartzite, biotite schist, and ultramafic schist. All of the rocks are intruded by mylonitic granite [10,11]. Iizuka et al. [5] carried out the geological mapping of the box area shown in Figure 1B and presented a 1:5000 geological map. They classified the major assemblage of foliated-to-gneissic rocks into four lithofacies: (1) a mafic–intermediate gneiss series, (2) a felsic gneiss series, (3) a layered gneiss series, and (4) foliated granite. The main mapped area is subdivided into two main domains by a northeast-trending fault, which juxtaposes contrasting lithologies (see Figure 3 of [5]). The felsic gneiss series occurs predominantly in the eastern area. The layered gneiss series is present mainly in the western area. The mafic–intermediate gneiss series predominantly occurs as enclaves of various sizes within the felsic gneiss. The foliated granite predominantly occurs in the western area as intrusions up to 200 m wide. The original igneous textures are preserved in the granite [5]. The zircon U–Pb geochronology conducted by Iizuka et al. [5] gives the foliated granite as 3.58 Ga, the layered gneiss series as 4.0–3.94 Ga and 3.73 Ga, the felsic gneiss series as 4.03–3.94 Ga, 3.74–3.72 Ga, 3.66 Ga, and 3.66–3.59 Ga, and the mafic–intermediate gneiss series as 4.0 Ga, >3.66 Ga, 3.6 Ga, and >3.59 Ga. These data suggest multiple zircon formations in the Acasta Gneiss Complex.

Guitreau et al. [6] summarized the geological events that occurred at the Acasta Gneiss Complex, as mentioned before.

Recently, Reimink and others have conducted analyses on various isotopes (O, U–Pb, Nd–Sm, W, Hf) and extinct nuclide and trace elements of zircon in the Acasta and related gneiss [12–15] and revealed (or found) (1) the oldest crust on Earth was generated from an older ultramafic or mafic reservoir on the earth surface; (2) the oxygen isotope compositions in Earth's mantle were homogenized by 4.02 Ga; (3) the crust production processes and spatial distribution of isotopic compositions imply a variable interaction with older crust; and (4) the Acasta Gneiss Complex is an appropriate analogue for the formation of the Hadean crust parental to the Jack Hills zircon grains.

Hildebrand et al. divided the Paleoproterozoic Wopmay orogen [16] into five major zones, ranging from east to west: the Coronation margin, the Turmoil klippe, the Medial zone, the Great Bear Magmatic Zone, and the Hottah terrane [17]. The rocks of the Coronation margin lie unconformably on the Archean rocks of the Slave craton and are collectively termed the Coronation Supergroup [18]. The U–Pb zircon geochronology of volcanic ash beds in the Supergroup provided an age of 1.961 Ga [19]. The rocks of the Turmoil klippe sit in thrust contact above the Coronation margin. The upper structural levels of the Turmoil klippe are dominated by a single thrust slice, consisting mostly of metamorphosed sedimentary rocks of the Akaitcho group. This group has U–Pb zircon ages of ca. 1.900–1.890 Ga [17]. Crystalline and cover rocks of the Akaitcho group within the Turmoil klippe have been perforated and intruded by plutons of the Hepburn intrusive suite [20]. These plutons having U–Pb zircon ages of ca. 1.900–1.880 Ga [17] are not known to intrude the underlying Slave craton and are confined to the Turmoil klippe. As discussed later, we think the relationship between these plutons and the basement gneisses is in situ. The Great Bear Magmatic Zone occupies most of the western exposed part of the Wopmay orogen and has U–Pb zircon ages of ca. 1.880–1.840 Ga [17]. The Medial zone occurs along the eastern margin of the Great Bear Magmatic Zone and includes rocks found in all the other zones [17]. Based on isotopic and field data, the western edge of the Slave craton lies within the Medial zone [21,22]. The Hottah terrane, which is exposed to the east and west of the Great Bear Magmatic Zone, consists of a crystalline basement, volcanic and sedimentary cover, and a variety of intrusive rocks; it has U–Pb zircon ages of ca. 1.960–1.930 Ga [17].

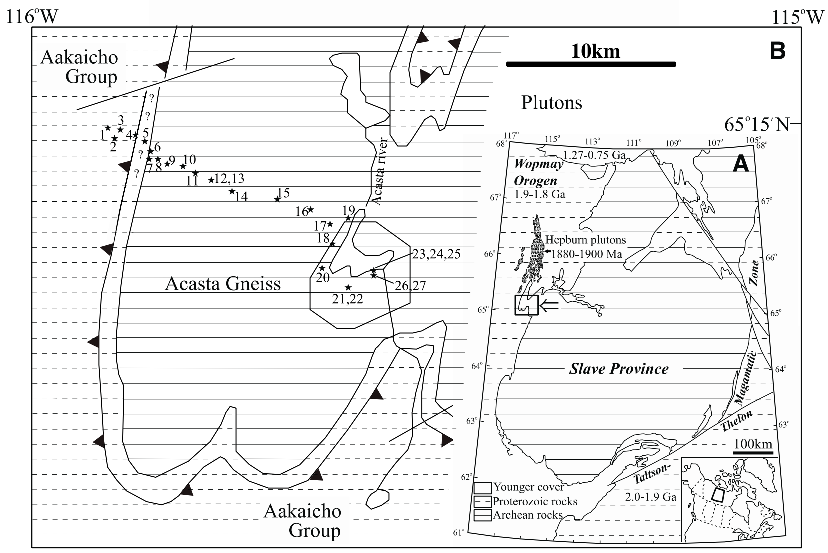

Figure 1. (**A**) a simplified geo-tectonic map of the Slave Province and its surroundings, taken from Hoffman [1]. The ages of Hepburn plutons are taken from Hildebrand et al. [17]. (**B**) a map showing

the locations of the studied samples. The barbed and solid lines in the lithological map represent the Proterozoic thrust and transcurrent faults, respectively [1,5]. The box shows the geological mapping area produced by Iizuka et al. [5]. The tonalitic gneiss used by Bowring et al. [3] was taken from the same location as samples 23, 24, and 25. A mark "?" zone (**B**) close to sample Hwp 5 belong to the Archean Acasta gneiss as explained in text.

3. Samples and Chemistry of Biotite and Amphibole

The Acasta gneisses and the Wopmay rocks were collected systematically along a traverse 18 km east–west stretch of the boundary between the Wopmay orogen and the Acasta gneiss (Figure 1B). Figure 1B shows the geological mapping area generated by Iizuka et al. [5]. The nine samples were collected from this geological mapping area. Five of these samples (Hwp 23, 24, 25, 26, and 27) were from the felsic gneiss series, which occurs predominantly in the eastern area (see Figure 3 of [5]). The tonalitic gneisses used by Bowring et al. [3] were from the area as mentioned above. All rock samples were collected from outcrops with the exposure of fresh rock, with few signs of weathering, as shown in a photograph (Figure 2). All of the samples are banded gneisses with distinct laminated textures. The gneisses were classified into three types petrographically: felsic, mafic, and intermediate (Figure S1). Figure 3 shows the photomicrographs of the representative rock samples: Hwp 2 (felsic) from the Akaitcho group of the Wopmay orogen and Hwp 14 (felsic) from the Acasta gneiss region. Hwp 2 contains coarse-grained plagioclase and quartz, and biotite. Hwp 14 contains rather smaller sized plagioclase and quartz, and biotite and amphibole as mafic minerals that are fresh without any secondary phases. No significant mineral zonation is observed optically. A mark "?" zone (Figure 1B) close to sample Hwp 5 (mafic) has been shown to belong to the Proterozoic Wopmay orogen (1,5). However, the zone may belong to the Archean Acasta gneiss because sample Hwp 5 contains amphibole like other Acasta gneiss, though the Wopmay samples (Hwp 1, 2, 3, and 4) do not. In this study, the barbed line (thrust) close to sample Hwp 5 is treated as the boundary between the Acasta gneisses and the Wopmay rocks. The Wopmay sample Hwp 4 (felsic) close to the thrust boundary consists of fine-grained minerals in comparison with that in samples Hwp 1 and Hwp 2 (felsic) far from the thrust boundary (Figure S1). Hwp 5 (mafic) also consists of fine-grained minerals in comparison with that in sample Hwp 23 (mafic) from the main Acasta gneiss region (Figure S1). This suggests these rocks have experienced grain size reduction by the deformation during thrust formation. This grain size reduction is observed in sample Hwp 4 (felsic) west of Hwp 5 and samples Hwp 6 (mafic) and Hwp 7 (felsic) east of Hwp 5 (Figure S1), indicating the size reduction zone reaches ca. 1 km width. The size reduction is also observed in samples Hwp 17 (felsic), Hwp 18 (felsic), Hwp 21 (felsic), and Hwp 22 (felsic) of the main Acasta gneiss area (Figure S1), suggesting the deformation to produce the mineral size reduction took place in several places.

The chemical compositions of biotite and amphibole were determined using an FESEM-EDS (JEOL JSM-7001F equipped with Oxford AZtec x-act Energy-Dispersive X-Ray Spectroscopy, Tokyo, Japan) operated at 15 kV accelerating voltage, a 1.4 nA beam current, and <3 µm beam spot size. Natural and synthetic silicates and oxides were used for calibration. Figure 4 shows the chemistry of biotite (Mg# [= Mg/(Mg + Fe^{2+})], Si, Ti, and K) and amphibole (Mg#, Si, Ti, and Na). The Mg# values of biotite from Wopmay range from 0.40 to 0.50. The values from Acasta range from 0.35 to 0.50 similar to the value from Wopmay except for significantly low-value samples. The Si values from Wopmay and Acasta are 2.65–2.70 and 2.60–2.75, respectively, showing no significant difference between them. The samples with low Mg# and Si values may indicate the substitution of Si (Mg, Fe)—(Al + Al). The Ti values from Wopmay and Acasta are 0.16–0.21 and 0.12–0.21, respectively. The K values are within a small variation from 0.73 to 0.81. The amphiboles in the Acasta gneisses consist of mainly clinoamphibole. One sample has exceptional orthoamphibole. The Mg# value of amphibole ranges from 0.5 to 0.8, suggesting the variable bulk composition of the gneiss. The Si values vary from 6.0 to 7.0 in relation with the Na values, suggesting some substitution of Si–(Na + Al). The Ti values are less than 0.2.

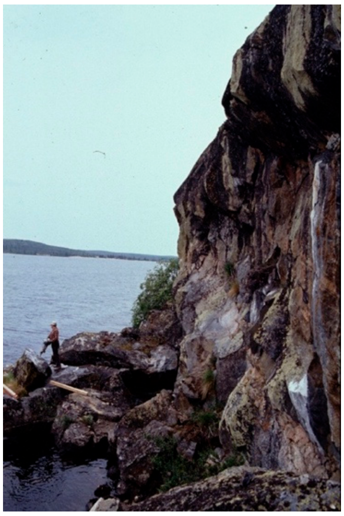

Figure 2. A photo of an outcrop of the Acasta gneiss by the Acasta River, close to the tonalitic gneiss used by Bowring et al. [3].

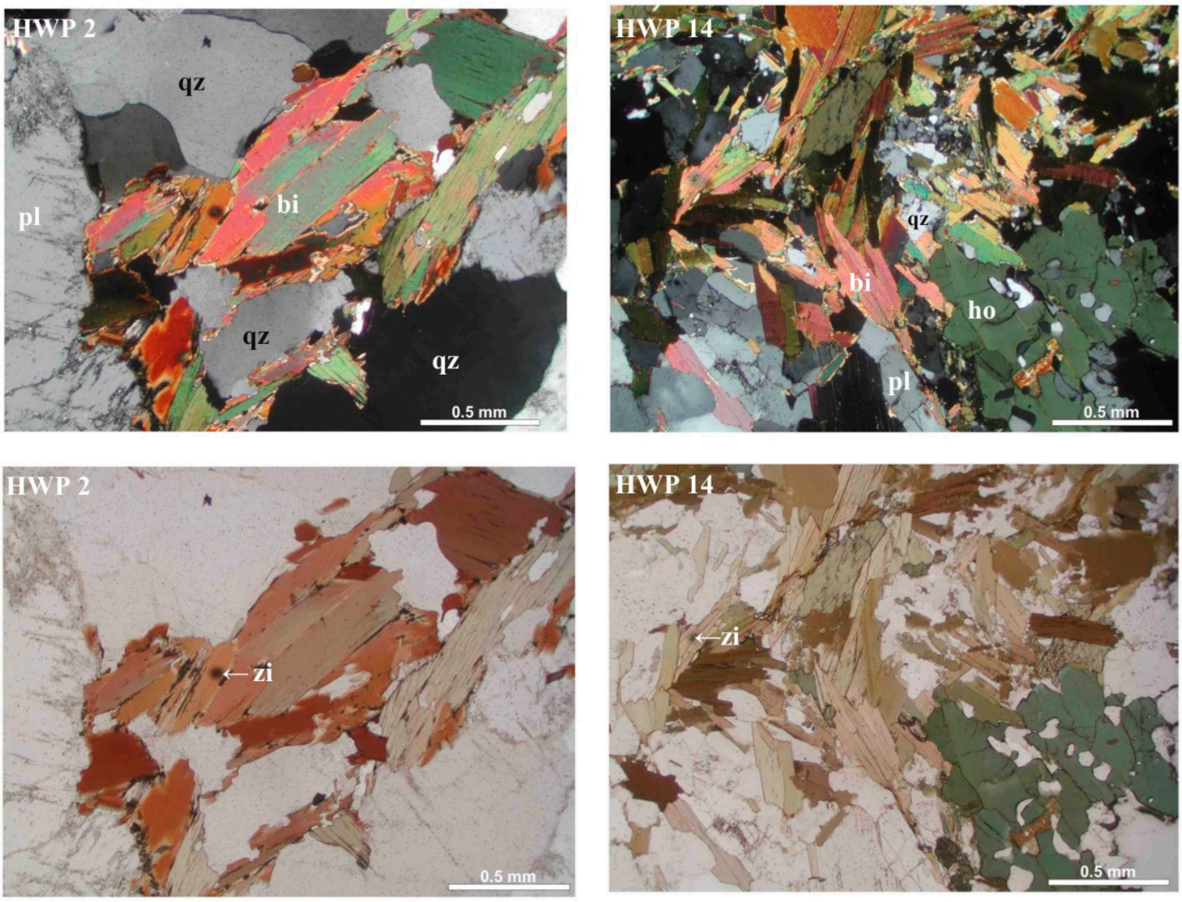

Figure 3. Photomicrographs of the representative rock samples: Hwp 2 is from the Akaitcho group of the Wopmay orogen and Hwp 14 is from the Acasta gneiss region.

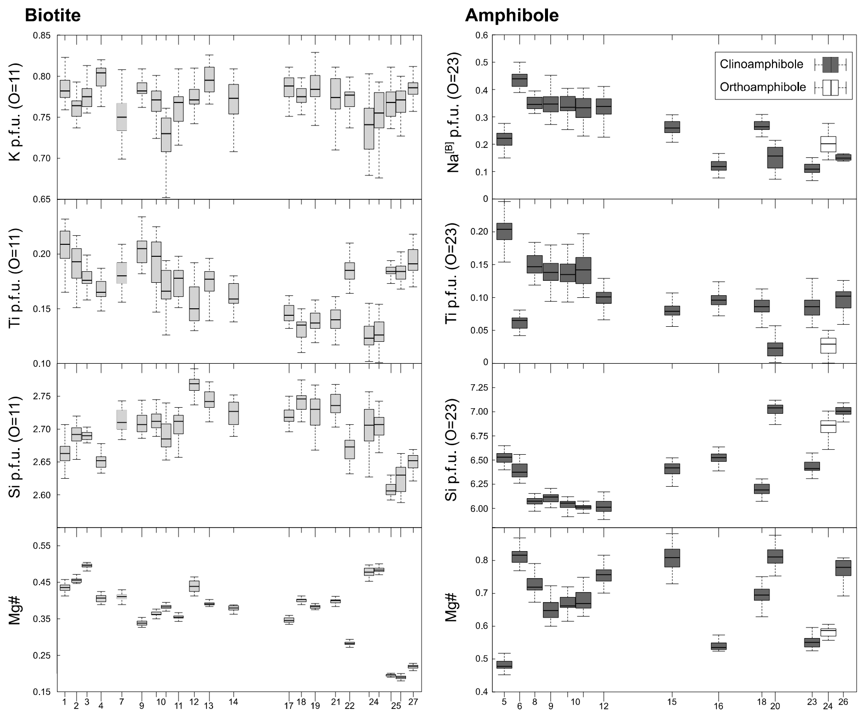

Figure 4. Chemistry of biotite and amphibole. Numerals of horizontal axis show sample numbers.

4. K–Ar Analyses

The samples were crushed and sieved, and the 30-to-50 mesh-size fraction was used for the separation of biotite and amphibole. The sieved fraction was washed in distilled water in an ultrasonic bath to remove fine particles on the grain surfaces and then dried in an oven at 80 °C. A clean, unaltered mineral sample was picked up under a stereomicroscope for the argon analyses. Separate aliquots were further pulverized in an agate mortar for potassium analysis. The potassium concentrations in the biotite and amphibole were determined using flame photometry [23]. Argon was analyzed at the Okayama University of Science using a sector-type mass spectrometer with a 15 cm radius and a single-collector, utilizing the isotope dilution and argon-38 spike methods [24]. Mass discrimination was checked with atmospheric argon each day. Specimens wrapped in Al foil were vacuumed out at ca. 180 °C for about 24 h, and argon was then extracted at 1500 °C in an ultra-high vacuum line. Reactive gases were removed using a Ti-Zr scrubber. The decay constants for ^{40}K to ^{40}Ar and ^{40}Ca, and the ^{40}K content in potassium was used in the age calculation, are 0.581×10^{-10}/y, 4.962×10^{-10}/y, and 0.0001167, respectively [25]. The K–Ar ages for the highly purified biotite and amphibole separates are listed in Table 1, in which the analytical error is at one sigma confidence level. Duplicate argon analyses were carried out for the biotite of Hwp 1, Hwp 9, and Hwp 14 and the amphibole of Hwp 11, Hwp 14, and Hwp 15. The results show a good reproducibility of the K–Ar analyses. The weighted average for these samples is also shown in Table 1. The ages are plotted along a traverse 18 km east–west stretch of the boundary between the Wopmay orogen and the Acasta gneiss (Figure 5).

The K–Ar biotite ages of the four Wopmay samples (Hwp 1, Hwp 2, Hwp 3, and Hwp 4) range from 1816 ± 18 Ma to 1854 ± 26 Ma, which is within the reported U–Pb zircon age range of the Wopmay orogen. The K–Ar biotite ages of the fifteen Acasta gneisses range from 1779 ± 25 Ma to 1877 ± 26 Ma (see Table 1), except for a younger Hwp 20 (1711 ± 25 Ma). The K–Ar amphibole ages range from 1685 ± 25 Ma to 1949 ± 19 Ma, giving a larger age variation in comparison with the biotite ages. The amphibole ages of Hwp 11 and Hwp 14 are higher than the zircon U-Pb age range (1880–1900 Ma) of Hepburn plutons (Figure 5), though these samples were affected by the Paleoproterozoic Wopmay orogeny. This is due to the fact that the amphiboles were not reset completely by the heating event, suggesting the temperature was not enough high to reset the amphibole. On the other hand, there are samples Hwp 6 (1685 ± 25 Ma), Hwp 15 (1737 ± 18 Ma), and Hwp 25B (1737 ± 27 Ma) that are significantly younger than the zircon U-Pb age range (1800–1900 Ma) of the Wopmay orogen. Although the exact reason is not known, it may be due to rejuvenation by local deformation.

Table 1. K–Ar age data of biotite and amphibole from the Akaitcho group of the Wopmay orogen and the Acasta gneisses. The distance is from sample Hwp 1. Duplicate argon analyses were carried out for the biotite of Hwp 1, Hwp 9, and Hwp 14 and the amphibole of Hwp 11, Hwp 14, and Hwp 15.

Sample	Potassium	Rad. ^{40}Ar	Age	Non-Rad. Ar	Distance	Rock Type	Long.	Lat.
	(wt.%)	(10^{-4} cc STP/g)	(Ma)	(%)	(km)			
Biotite								
Hwp 1	7.332	8.946	1810 ± 26	0.2	0.0	felsic	115°54′16.02″ W	65°14′27.19″ N
		9.259	1821 ± 26	0.3	0.0		′	
		Weighted average	1816 ± 18					
Hwp 2	6.461	7.995	1837 ± 26	0.4	0.6	felsic	115°53′46.11″ W	65°14′7.40″ N
Hwp 3	7.755	9.559	1832 ± 26	0.5	0.7	felsic	115°53′21.81″ W	65°14′23.83″ N
Hwp 4	7.769	9.757	1854 ± 26	0.4	1.7	Int.	115°52′6.45″ W	65°14′15.97″ N
Hwp 9	7.122	9.185	1884 ± 26	0.3	4.1	felsic	115°50′22.68″ W	65°13′31.01″ N
		8.856	1842 ± 26	0.3	4.1			
		Weighted average	1863 ± 18					
Hwp 11	7.462	9.562	1877 ± 26	0.4	5.9	Int.	115°47′28.12″ W	65°13′3.37″ N
Hwp 12	7.217	8.642	1799 ± 25	0.3	7.0	felsic	115°46′12.91″ W	65°12′51.39″ N
Hwp 13	7.935	9.535	1803 ± 26	0.4	7.0	felsic	115°46′12.91″ W	65°12′51.39″ N
Hwp 14	7.227	8.615	1794 ± 25	0.5	8.3	felsic	115°44′34.80″ W	65°12′31.59″ N
		8.773	1814 ± 26	0.3	8.3			
		Weighted average	1804 ± 18					
Hwp 17	7.562	9.329	1833 ± 26	0.3	14.5	Int.	115°37′1.12″ W	65°11′31.66″ N
Hwp 18	6.987	8.518	1819 ± 26	0.2	15.0	Int.	115°36′49.07″ W	65°10′53.86″ N
Hwp 19	7.142	8.547	1789 ± 26	0.2	15.0	felsic	115°35′39.35″ W	65°11′46.60″ N
Hwp 20	6.680	7.397	1711 ± 25	0.1	15.4	mafic	115°37′34.09″ W	65°10′5.66″ N
Hwp 21	6.521	7.889	1811 ± 26	0.2	16.6	felsic	115°35′31.20″ W	65° 9′31.14″ N
Hwp 22	7.103	8.711	1826 ± 26	0.2	16.6	felsic	115°35′31.20″ W	65° 9′31.14″ N
Hwp 23	5.532	6.745	1819 ± 26	0.1	17.9	mafic	115°33′37.14″ W	65°10′4.40″ N
Hwp 24A	6.472	7.751	1798 ± 25	0.2	17.9	mafic	115°33′37.14″ W	65°10′4.40″ N
Hwp 26	7.877	9.854	1789 ± 25	0.1	17.9	Int.	115°33′35.75″ W	65° 9′54.76″ N
Hwp 27	6.907	8.129	1779 ± 25	0.2	17.9	mafic	115°33′35.75″ W	65° 9′54.76″ N
Amphibole								
Hwp 5	0.627	0.768	1824 ± 26	0.9	2.3	mafic	115°51′25.82″ W	65°14′2.59″ N
Hwp 6	0.274	0.296	1685 ± 25	2.3	2.9	mafic	115°50′54.73″ W	65°13′43.43″ N
Hwp 8	1.114	1.383	1840 ± 26	0.5	3.4	Int.	115°50′22.68″ W	65°13′31.01″ N
Hwp 9	0.952	1.200	1858 ± 26	0.5	4.1	felsic	115°50′22.68″ W	65°13′31.01″ N
Hwp 10A	0.948	1.201	1863 ± 26	0.4	5.1	Int.	115°48′22.87″ W	65°13′16.16″ N
Hwp 11	1.178	1.608	1952 ± 27	0.5	5.9	Int.	115°47′28.12″ W	65°13′3.37″ N
		1.599	1945 ± 27	0.4	5.9		115°47′28.12″ W	65°13′3.37″ N
		Weighted average	1949 ± 19					
Hwp 12	1.262	1.647	1899 ± 26	0.4	7.0	felsic	115°46′12.91″ W	65°12′51.39″ N
Hwp 14	1.269	1.705	1933 ± 27	0.4	8.3	felsic	115°44′34.80″ W	65°12′31.59″ N
		1.676	1913 ± 26	0.3	8.3		115°44′34.80″ W	65°12′31.59″ N
		Weighted average	1923 ± 19					
Hwp 15	0.482	0.556	1756 ± 25	0.5	10.9	Int.	115°41′9.07″ W	65°12′17.52″ N
		0.537	1718 ± 25	0.3	10.9		115°41′9.07″ W	65°12′17.52″ N
		Weighted average	1737 ± 18					
Hwp 16	0.833	1.056	1864 ± 26	0.7	12.9	mafic	115°38′33.82″ W	65°11′59.46″ N
Hwp 18	1.947	2.309	1788 ± 26	0.3	15.0	Int.	115°36′49.07″ W	65°10′53.86″ N
Hwp 25B	0.420	0.476	1737 ± 27	0.4	17.9	felsic	115°33′37.14″ W	65°10′4.40″ N

It should be noted that Hwp 9 and Hwp 18 have biotite older than amphibole, though Hwp 12 has biotite younger than amphibole. The closure temperature of the K-Ar biotite and amphibole system may have compositional dependence cf. [26]. Its understanding so far is given in Appendix A. The age difference between biotite and amphibole in Hwp 18 is 31 million years (Tables 1 and 2). This difference requires the closure temperature of biotite to be at least 300 °C higher than that of amphibole when the cooling rate of the rock was 10 °C/Myr. Reducing the cooling rate also lowers the closure temperature but only to bring it closer to that of amphibole. It is hard to make biotite older than amphibole using the compositional dependence which is not significant (see Appendix A). An alternative possible reason is that the biotite trapped the excess argon wave (see Appendix B) generated in nearby minerals and/or rocks. Compared to Hwp 12, Hwp 18 is composed of fine-grained minerals (Figure S1). This grain size reduction by deformation may be related to the generation of excess argon waves. The specific trapping mechanism is not well understood but inferred from Figure A3 in Appendix B. We suggest that the trapping of argon by biotite in the excess argon wave took place when the rocks cooled down to temperatures lower than the closure temperature of amphibole but not below that of biotite.

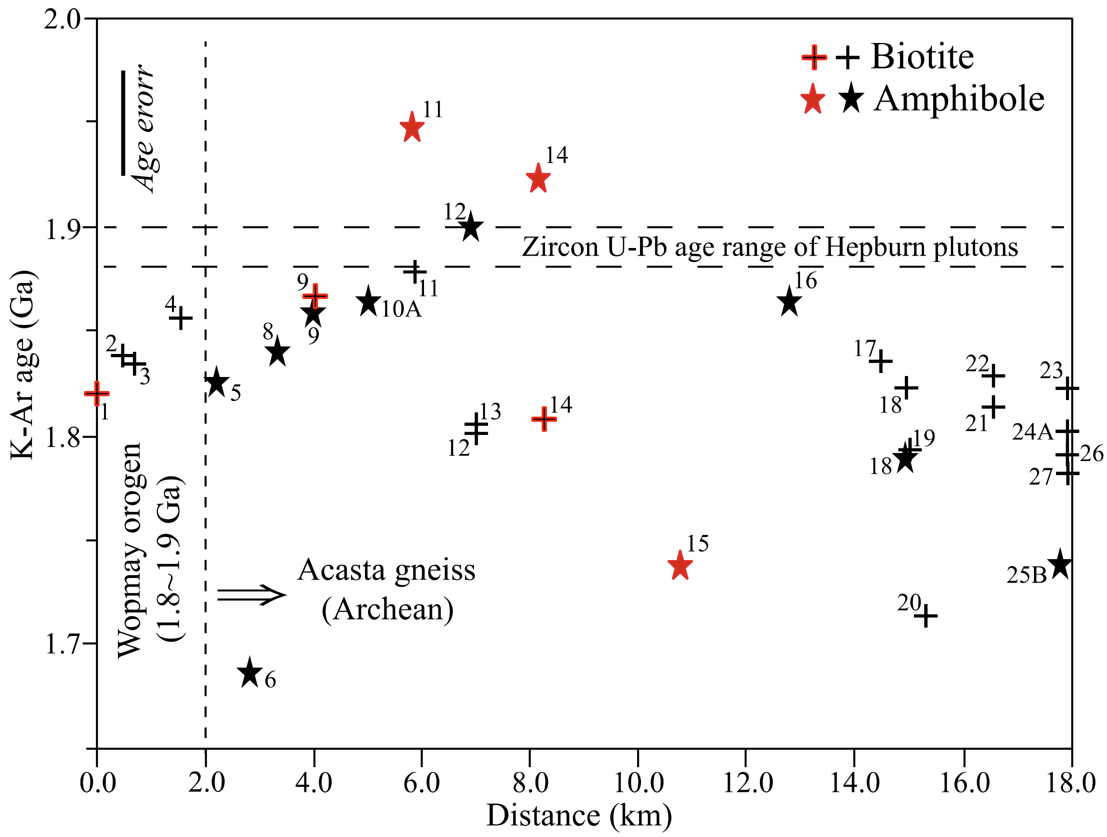

Figure 5. Ages plotted along a traverse 18 km east–west stretch of the boundary between the Wopmay orogen and the Acasta gneiss. The error of each age is within the range of the error bar shown in the figure. Duplicate argon analyses were carried out for the biotite of Hwp 1, Hwp 9, and Hwp 14 and for the amphibole of Hwp 11, Hwp 14, and Hwp 15. The weighted average for these samples is shown in red. The error is halved from the age error bar.

Table 2. A summary table comparing all of the ages of the samples, K-Ar age, and $^{40}Ar/^{39}Ar$ total gas age and plateau age. Two crystals (a and b) from Hwp 12 were analyzed.

Sample	Mineral	K-Ar Age	$^{40}Ar/^{39}Ar$	$^{40}Ar/^{39}Ar$
		Ma	Total gas age (Ma)	Plateau age (Ma)
Hwp 1	biotite	1816 ± 18	1820 ± 21	1826 ± 21
Hwp 2	biotite	1837 ± 26	1885 ± 13	1886 ± 13
Hwp 3	biotite	1832 ± 26		
Hwp 4	biotite	1854 ± 26	1866 ± 18	1870 ± 18
Hwp 5	amphibole	1824 ± 26	1789 ± 23	1814 ± 22
Hwp 6	amphibole	1685 ± 25		
Hwp 8	amphibole	1840 ± 26		

Table 2. *Cont.*

Sample	Mineral	K-Ar Age	$^{40}Ar/^{39}Ar$	$^{40}Ar/^{39}Ar$
Hwp 9	biotite	1863 ± 18		
Hwp 10A	amphibole	1858 ± 26	1648 ± 45	
	amphibole	1863 ± 26	1580 ± 68	
Hwp 11	biotite	1877 ± 26	1709 ± 49	
	amphibole	1949 ± 19	1598 ± 126	
Hwp 12	biotite	1799 ± 25	1994 ± 9	
	amphibole	1899 ± 26	(a) 1827 ± 14	(a) 1847 ± 15
			(b) 1839 ± 33	
Hwp 13	biotite	1803 ± 26		
Hwp 14	biotite	1804 ± 18	1817 ± 8	1877 ± 8
	amphibole	1923 ± 19	1948 ± 24	
Hwp 15	amphibole	1737 ± 18	1731 ± 73	
Hwp 16	amphibole	1864 ± 26	1683 ± 66	
Hwp 17	biotite	1833 ± 26		
Hwp 18	biotite	1819 ± 26	1907 ± 12	1935 ± 14
	amphibole	1788 ± 26	2127 ± 10	
Hwp 19	biotite	1789 ± 26		
Hwp 20	biotite	1711 ± 25		
Hwp 21	biotite	1811 ± 26		
Hwp 22	biotite	1826 ± 26		
Hwp 23	biotite	1819 ± 26		
Hwp 24A	biotite	1798 ± 25		
Hwp 25B	biotite		1939 ± 8	1951 ± 11
	amphibole	1737 ± 27	1967 ± 11	1964 ± 12
Hwp 26	biotite	1789 ± 25		
Hwp 27	biotite	1779 ± 25		

5. Laser Step-Heating $^{40}Ar/^{39}Ar$ Analyses

$^{40}Ar/^{39}Ar$ analyses of biotite and amphibole were carried out using the temperature-controlled laser step-heating method [27–29]. Each mineral grain (ca. 0.5 mm in size) was placed in a 2 mm drill hole on an aluminum tray, together with a standard-age grain (3gr amphibole; [30]), and calcium ($CaSi_2$) and potassium (synthetic $KAlSi_3O_8$ glass) salts for the Ca and K corrections, respectively. Subsequently, the trays were vacuum-sealed in a quartz tube. The neutron irradiation of the sample was carried out in the core of the 5 MW Research Reactor at Kyoto University (KUR) for 8 h using the hydraulic rabbit facility (a sample-capsule transferring system with hydraulic pressure). The fast neutron flux density was 3.9×10^{13} n/cm^2/s and was confirmed to be uniform in the dimension of the sample holder (φ16 mm × 15 mm), as little variation in the J-values of the evenly spaced age standards was observed [27]. The J-values are shown in Table S1. The potassium and calcium correction factors are (40/39) K = 0.0155 ± 0.0030, (36/37) Ca = 0.000256 ± 0.000028, and (39/37) Ca = 0.000847 ± 0.000020, respectively.

Each mineral was analyzed with the step-heating technique using a 5 W continuous argon ion laser. The temperatures of the samples were monitored using an infrared thermometer with a precision of 3° within an area of 0.3 mm in diameter [28]. The single crystal was heated under a defocused laser beam at a given temperature for 30 s. The extracted gas was purified using a SAES Zr-Al getter (St 101) and kept at 400 °C for 5 min. Argon isotopes were measured using a custom-made mass spectrometer with a high resolution ([M/ΔM] = ca. 800), which allowed for the separation of hydrocarbon peaks, except for mass 36 [29]. Typical blanks of the extraction lines are 4×10^{-11}, 2×10^{-13}, 3×10^{-14}, and 8×10^{-9} ccSTP for ^{36}Ar, ^{37}Ar, ^{39}Ar, and ^{40}Ar, respectively. The ^{40}Ar/^{39}Ar analyses data are shown in Table S1. The age spectra and $^{37}Ar_{Ca}/^{39}Ar_{K}$ ratios of the analyzed samples are shown in Figure 6. Table 2 is a summary table comparing all of the ages of the samples, K-Ar age, and ^{40}Ar/^{39}Ar total gas age and plateau age.

As seen in Figure 6 and Table 2, the ^{40}Ar/^{39}Ar biotite analyses of the three samples (Hwp 1, Hwp 2, and Hwp 4) from the Wopmay orogen give the plateau ages 1826 ± 21 Ma, 1886 ± 13 Ma, and 1870 ± 18 Ma, respectively. These plateau ages are the same as the total gas ages within the analytical error. However, the K–Ar biotite age (1837 ± 26 Ma) of Hwp 2 is a little younger than the ^{40}Ar/^{39}Ar plateau age (1886 ± 13 Ma), suggesting that some biotite grains experienced argon loss. On the other hand, the ^{40}Ar/^{39}Ar analyses of the biotite crystals from the Acasta gneiss show a variety of ages. Hwp 14, Hwp 18, and Hwp 25B show the plateau ages of 1877 ± 8 Ma, 1935 ± 14 Ma, and 1951 ± 11 Ma, respectively. The latter two samples (Hwp 18 and Hwp 25B) are a little older than the zircon U-Pb ages (1880–1900 Ma) of the Hepburn plutons, though their K-Ar ages are significantly younger (Table 2). This is because, by chance, crystals with excess argon were chosen for the analysis. The total gas age (1994 ± 9 Ma) of Hwp 12 is significantly older than the K–Ar age (1799 ± 25 Ma). This may also be because an excess argon-bearing crystal was, by chance, chosen for the analysis. This crystal appears to be significantly older than 2000 Ma in the middle temperature fraction. This suggests that the biotite crystal happened to trap the excess argon wave generated in nearby minerals and/or rocks as described before. This indicates that the Acasta gneiss originally contained biotite. The ^{40}Ar/^{39}Ar analyses of the amphibole crystals show more varied age relations. Hwp 5 and Hwp 25B show consistent age relations between the plateau ages (1814 ± 22 Ma and 1964 ± 12 Ma) and the total gas ages (1789 ± 23 Ma and 1967 ± 11 Ma), respectively. Two crystals from Hwp 12 were analyzed. Crystal (a) shows consistent age relations between the plateau ages (1847 ± 15 Ma) and the total gas ages (1827 ± 14 Ma). Crystal (b) shows no plateau age spectra and gives a total gas age of 1839 ± 33 Ma, which is similar to the age of the crystal (a). This crystal has the apparent old age of 2000 Ma in the middle temperature fractions. The crystal of Hwp 14 also has fractions older than 2000 Ma. These old fractions result from the amphibole crystals, originally formed in the Archean, being affected by thermal events during the Wopmay orogeny, but not completely reset.

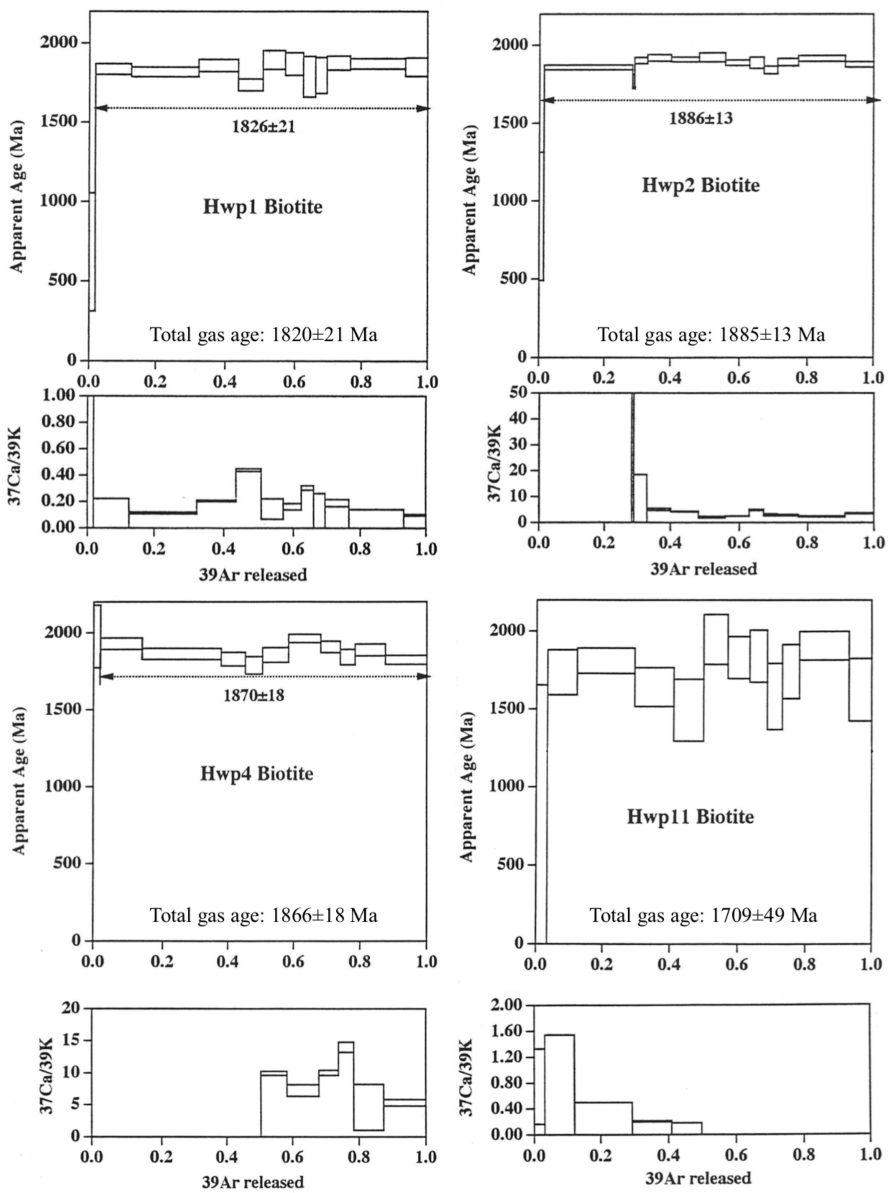

Figure 6. *Cont.*

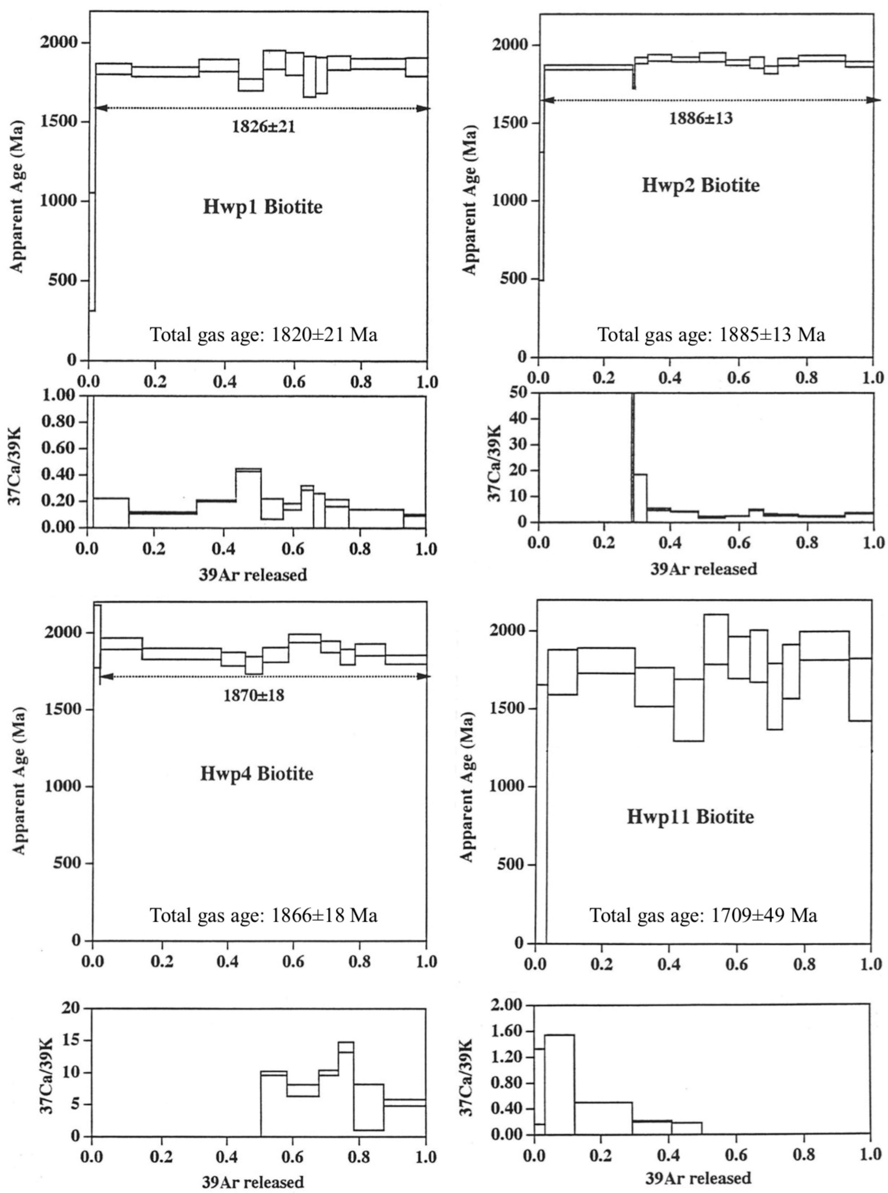

Figure 6. *Cont.*

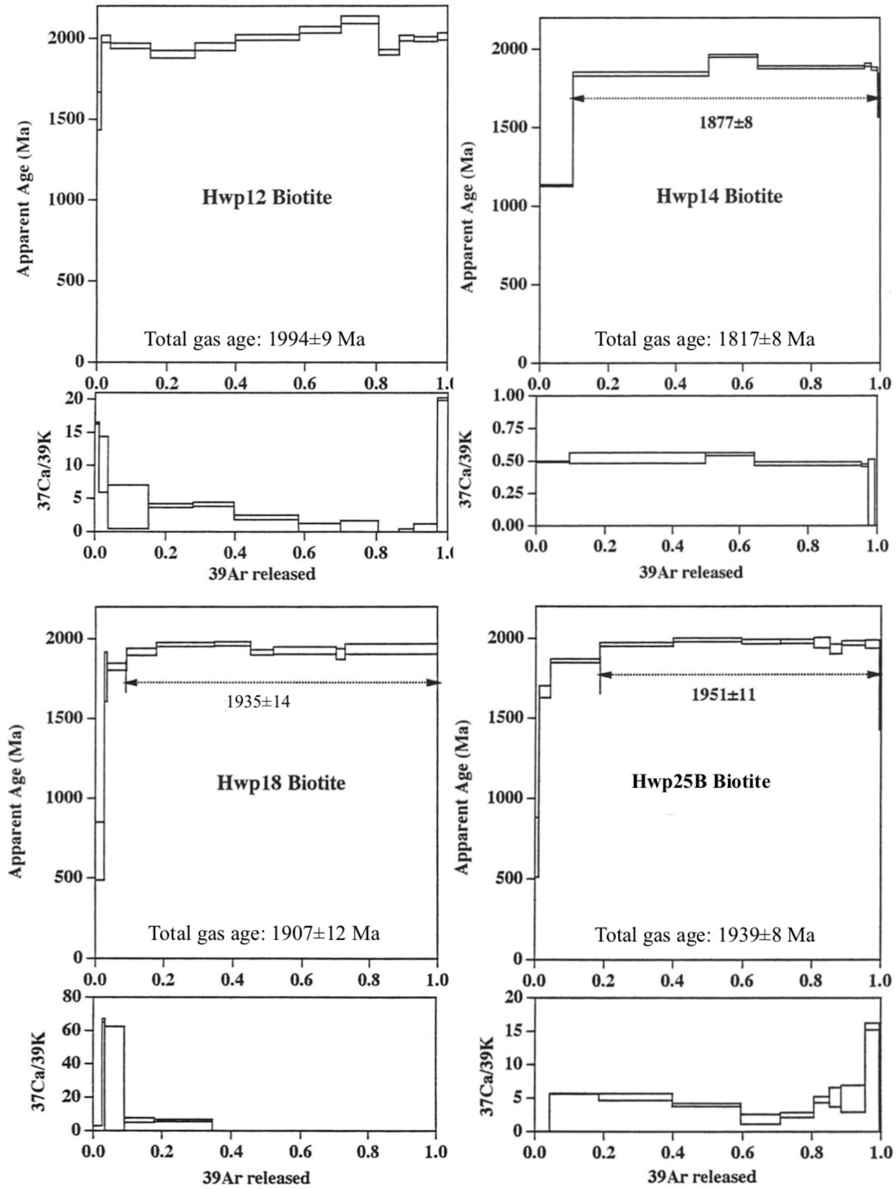

Figure 6. *Cont.*

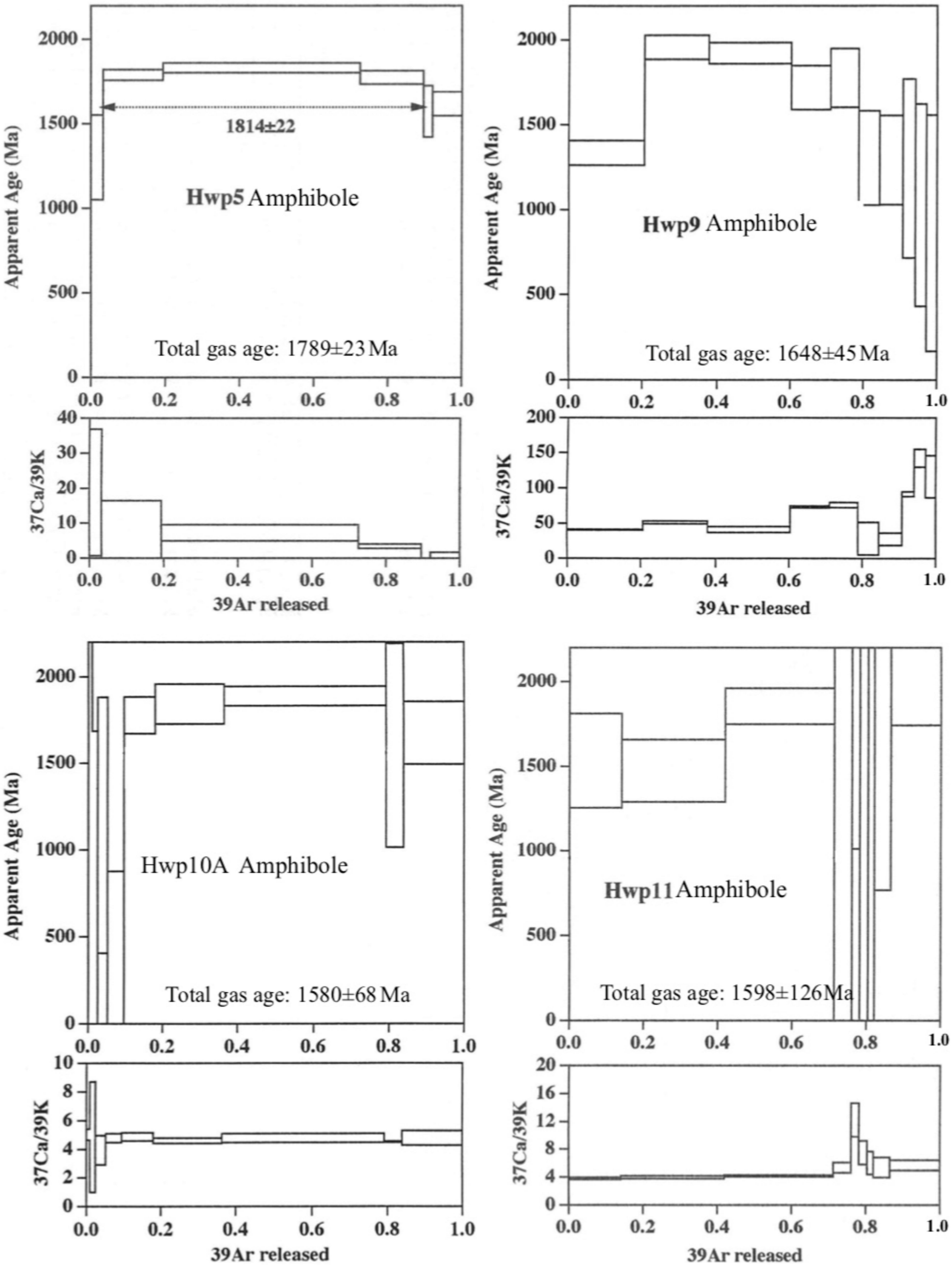

Figure 6. *Cont.*

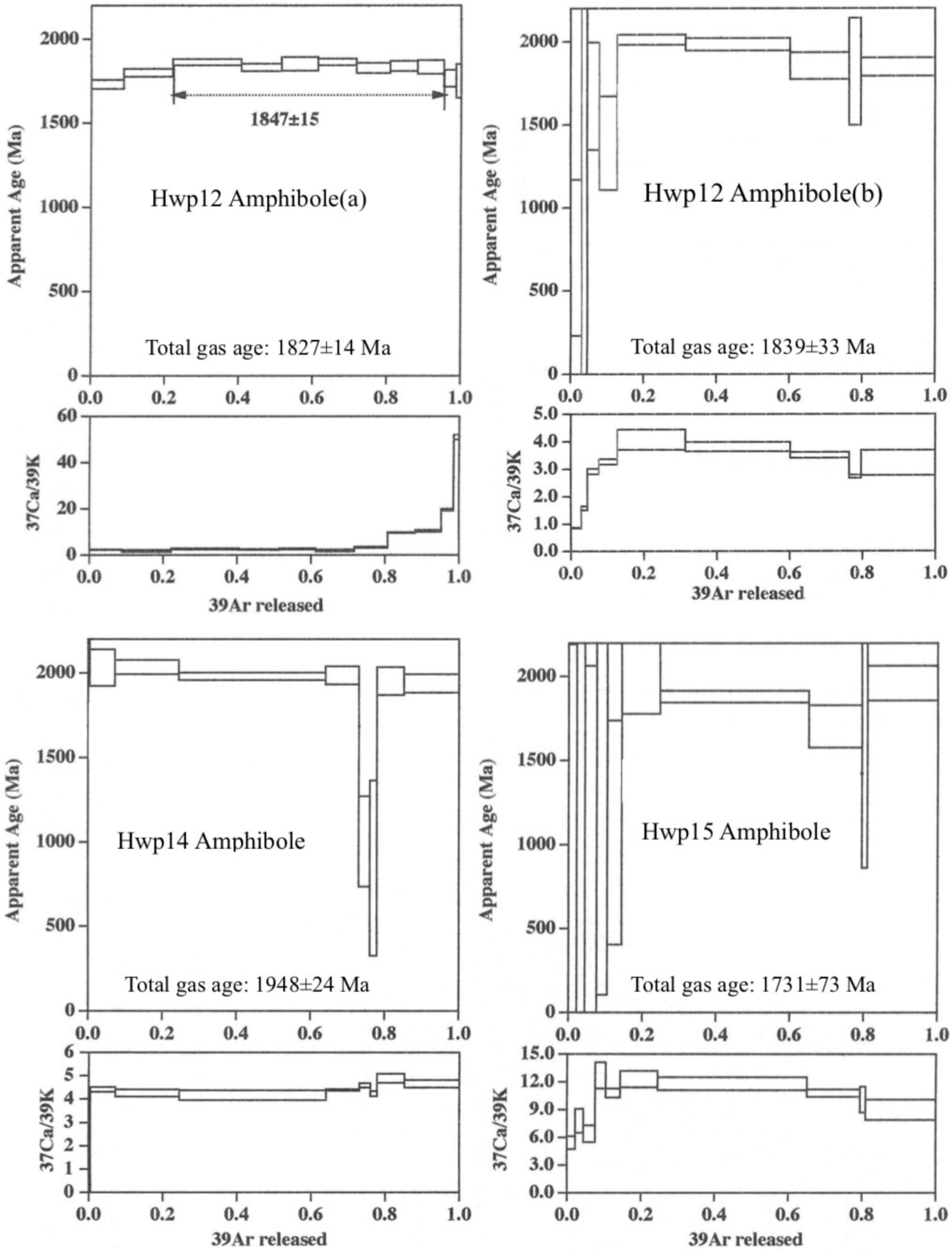

Figure 6. *Cont.*

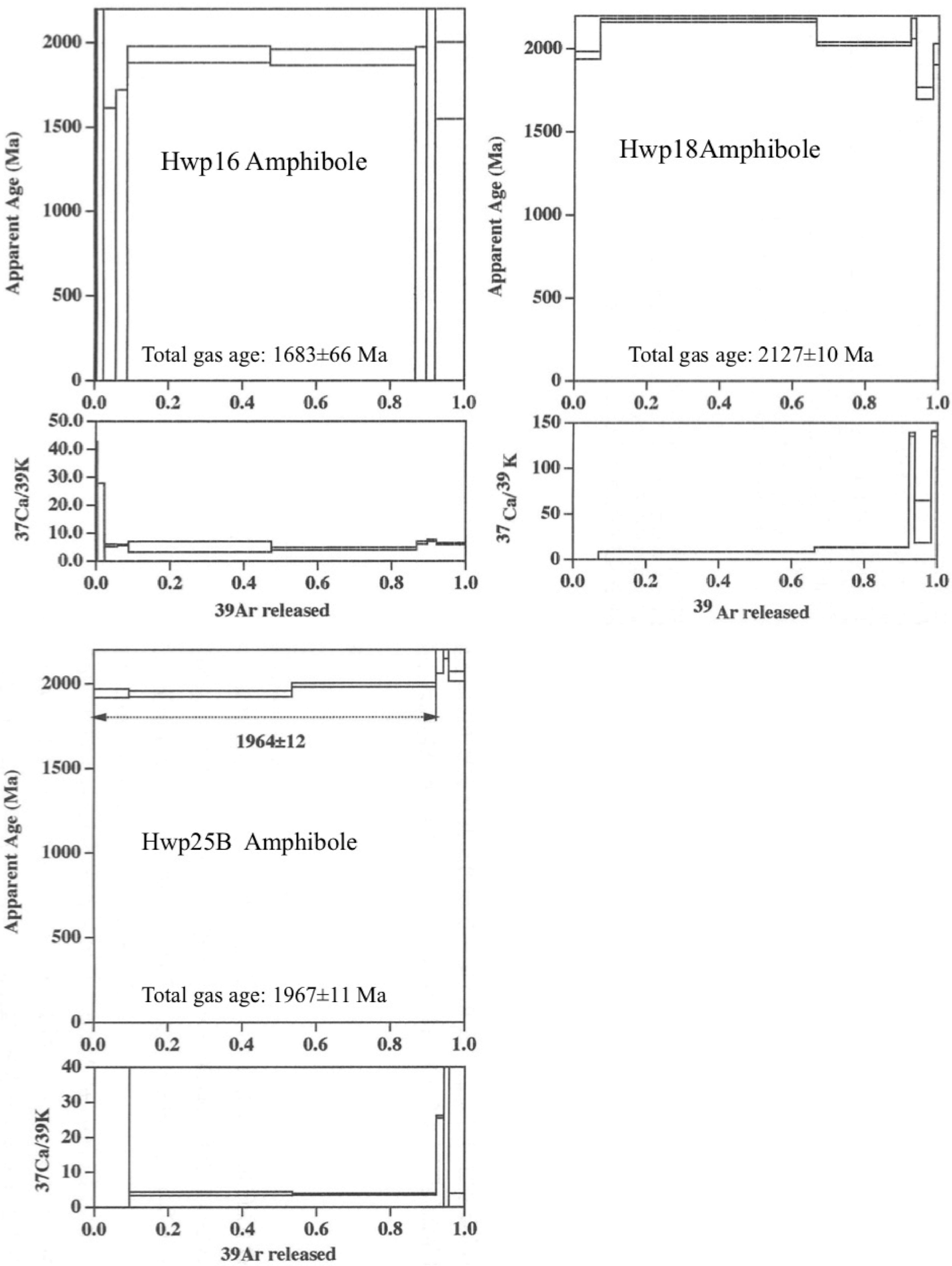

Figure 6. The age spectra and $^{37}Ar_{Ca}/^{39}Ar_K$ ratios of the samples from the Wopmay orogen and the Acasta gneisses. When the analytical error of the $^{37}Ar_{Ca}/^{39}Ar_K$ ratios of some fractions from biotite was large enough (see Table S1), we did not draw the ratios. A plateau was defined as where successive ^{39}Ar fractions coincide within a margin of error (1 sigma) and occupy more than 80% of the total release. The error of the calculated plateau age is at one sigma confidence level.

6. Discussion

6.1. Wopmay Orogen Event on Archean Acasta Gneiss Complex

Based on zircon U–Pb geochronology, Guitreau et al. [6] summarized the geological events that occurred at the Acasta Gneiss Complex, showing multi-stage events such as the crystallization of the zircon core (4.2 Ga), the formation of the oldest diorites and tonalities, the tonalite formation, the granodiorite formation and the associated anatexis, the regional metamorphism with granitoid formation, and the granite intrusion (2.6 Ga), as described before. They also proposed the Wopmay orogen event using the $^{40}Ar/^{39}Ar$ ages of biotite and amphibole presented by Hodges et al. [7]. We confirmed more clearly the existence of the Wopmay orogen event based on K–Ar and $^{40}Ar/^{39}Ar$ analyses of biotite and amphibole from the Acasta gneisses. This is an event that rejuvenated the K–Ar system ages of the biotite and amphibole of the Archean gneiss to the Paleoproterozoic ages. This rejuvenation worked to reset the K–Ar systems of biotite and amphibole. The resetting of the white mica K–Ar system in the collisional orogenic belts is not always completed during high-pressure (HP)–ultra-high-pressure (UHP) metamorphism (cf. [31] and references therein). This is because white mica has a high closure temperature (ca. 600 °C and above). Itaya et al. [32] presented a variation diagram of the closure temperature of the biotite K–Ar system for different grain sizes and cooling rates based on the diffusion model proposed by Dodson [33]. The diagram indicates that the closure temperature is ca. 420 °C under a grain size of 1 mm and a cooling rate of 1000 °C/Myr. A slower cooling rate and smaller grain size further reduce the closure temperature. The closure temperature of amphibole has been described as ca. 500 °C [34]. The closure temperature of the zircon U–Pb system depends on the nature of the zircon grains. Sano et al. [35] posited that it is ca. 880 °C when discussing the cooling history of the Acasta gneiss. These closure temperature relations mean that the thermal effect of the Wopmay orogen event must be 500–880 °C. This is because amphibole has been rejuvenated but zircon has not.

6.2. Paleoproterozoic Hepburn Batholith

The Coronation Supergroup described by Hildebrand et al. [17] that lies to the east of the "Turmoil klippe" was deformed and metamorphosed [1,36]. The metamorphic grade increases toward the Hepburn batholith from the eastern side, as revealed by the mineral zone distribution, namely the chlorite, biotite, aluminosilicate, and K-feldspar zones [16]. This mineral paragenesis suggests the metamorphism of the low P/T type. The garnet–biotite geothermometry in the pelitic rocks close to the Hepburn batholith gave the highest temperature of 765 °C [37]. The plutonic suit comprised more than 200 discrete plutons ranging widely in size, composition, tectonic fabric, and the level of emplacement [16]. The largest and most abundant intrusions are variably foliated and megacrystic, typically containing metasedimentary xenoliths, accessory garnet, and sillimanite. The granites are peraluminous and have low magnetic susceptibility and moderately heavy whole-rock oxygen isotope ratios of δO18 = 8 to 13 [38]. These characteristics imply a strong metasedimentary contribution by anatexis [16]. This situation is similar to that of the Cretaceous Ryoke metamorphic belt in southwest Japan and the Tia Complex in the southern New England Fold Belt, Australia: both consisting of the typical Pacific-type orogenic belts. The Ryoke belt comprises a Jurassic accretionary complex with Cretaceous Ilmenite-series peraluminous granite [39,40]. The metamorphic grade of the metamorphosed complex increases from north to south where the migmatite zone is 700–850 °C [41]. Migmatite has drawn attention as a possible source for granitic magma. It has been speculated that anatectic melts are extracted from it and segregated to grow and coalesce, forming a pluton-sized magma body (e.g., [42–44]). We suggest that the peraluminous granitoids have been formed by the partial melting of the subduction–accretion complex that suffers the low P/T-type metamorphism with heating by a specific magma produced in the wedge mantle. Cretaceous high-Mg andesites, adakites, and high-Nb basalts have been observed in SW Japan [45,46]. This type of magma is distinct from the typical arc magma produced during the active subduction of oceanic plates. We consider that the Ryoke metamorphic rocks and the associated peraluminous granitic rocks were formed with heating by specific magma because the ages of the metamorphic rocks, granitic rocks, and the volcanic rocks are consistent with each other. These specific magmas could be formed by the tectonic change in the wedge mantle such as the rollback or shift back of the subducting slab of the oceanic plate and the subsequent upwell of the high-T asthenosphere into the wedge mantle. In the Tia Complex, the early Carboniferous subduction complex suffered the low P/T-type of metamorphism in Permian with heating by the specific magma. At that time, the S-type granitoids of the Hillgrove suite formed (see Figure 3 of [47]). The Hepburn batholith and the associated low P/T-type of metamorphic rocks would be also due to heating by the specific magma that took place in the Paleoproterozoic. This specific magma would form when the high-T asthenosphere introduces into the wedge mantle by the rollback or shift back of the subducting slab of the oceanic plate as proposed by the study of the Ryoke belt in SW Japan.

6.3. Heat Source Affecting the Acasta Gneiss

The Hepburn plutons extend along the north–south direction (Figure 1A). It is probable that an asthenospheric intrusion occurred in a strip along this direction. This suggests that the specific magma formed by asthenospheric intrusion would also occur below the Acasta gneiss that exists on the extension of the N-S-extending Hepburn plutons. This specific magma could have a thermal effect on the Acasta gneiss, rejuvenating the K–Ar system ages of biotite and amphibole. The biotite K–Ar ages of the samples (Hwp 23, Hwp 24, Hwp 26, and Hwp 27) 16 km away from the boundary between the Wopmay orogen and the Acasta gneiss are the same as the ages of the Wopmay rocks within the analytical error (Figure 5). These results indicate that the extent of the thermal effect is at least 16 km laterally away from the asthenospheric intrusion axis. This extent is comparable with the width of the Hepburn plutons.

The biotite in the Acasta gneisses seems to have been reset to a significant degree by the thermal effect of the specific magma (Figures 5 and 6). However, amphibole crystals are not always completely reset. As seen in Figure 6, the amphibole crystal (a) of Hwp 12 gives consistent age relations between the plateau ages (1847 $\pm$ 15 Ma) and the total gas ages (1827 $\pm$ 14 Ma), suggesting it was reset completely. The crystal (b) from the same sample shows no plateau age spectra and has the apparent old age of 2000 Ma in the middle temperature fraction. The amphibole crystal of Hwp 14 also has fractions older than 2000 Ma (Figure 6). As described before, the K-Ar amphibole's ages of Hwp 11 and Hwp 14 are older than the zircon U-Pb ages (1880–1900 Ma) of Hepburn plutons (Figure 5). This suggests the thermal effect took place around the closure temperature of amphibole, and the temperature around the area of samples Hwp 11, Hwp 12, and Hwp 14 was not high enough to reset the amphiboles completely.

7. Summary

Slave Province is a well-exposed Archean terrane located in the northwestern corner of the Canadian Shield. It is bordered by the Thelon–Taltson orogenic belt (2.0 to 1.9 Ga) to the southeast and the Wopmay orogenic belt (1.9 to 1.8 Ga) to the west. The Acasta gneisses are exposed along the Acasta River in the westernmost part of Slave Province. The zircon U–Pb geochronology of the gneisses has been undertaken since the discovery of the 3.96 Ga gneiss in 1989, revealing multi-stage events from 4.2 to 2.6 Ga. The Wopmay orogen event has also been proposed to have occurred from the $^{40}Ar/^{39}Ar$ age of biotite and amphibole. We confirmed with greater certainty the existence of the Wopmay orogen event based on K–Ar and $^{40}Ar/^{39}Ar$ analyses of biotite and amphibole from Acasta gneisses, which were collected systematically along an 18 km east–west traverse of the boundary between the Wopmay orogen and the Acasta gneiss. This is an event that rejuvenated the K–Ar system ages of the biotite and amphibole of the Archean gneiss to the Paleoproterozoic ages. The heat source that rejuvenated the K–Ar system ages could be the specific magma formed by the high-T asthenosphere intrusion into the wedge mantle due to the rollback or shift back of the subducting slab of the oceanic plate.

Supplementary Materials: The following supporting information can be downloaded at: https://www.mdpi.com/article/10.3390/min14040397/s1, Figure S1: Photomicrographs (crossed polars) of the Wopmay rocks and the Acasta gneisses.; Table S1: $^{40}Ar/^{39}Ar$ analyses data.

Author Contributions: Conceptualization, T.I. and H.H.; methodology, T.I. and H.H.; software, H.H.; resources, T.I. and H.H.; K–Ar and $^{40}Ar/^{39}Ar$ analyses; M.S. and H.H.; EMP analyses, K.S.; writing—original draft preparation, M.S. and H.H.; writing—review and editing, T.I., H.H. and T.T.; supervision and project administration, T.I. All authors have read and agreed to the published version of the manuscript.

Funding: This research was partly supported by the Earth History Project led by S. Maruyama.

Data Availability Statement: The data presented in this study are available in Supplementary Materials.

Acknowledgments: The neutron irradiation experiment was carried out as part of the visiting researcher program in Kyoto University Reactor (KUR). We thank the staff of Kyoto University and especially K. Takamiya for his help during the course of the experiment. H.H. also thanks P.F. Hoffman and the late S.A. Bowring for their guidance in the Acasta area and C.E. Isachsen, M. Arima, H. Sakai, Y. Koide, and H. Baba for their help in the field. The sampling was partly supported by the Earth History Project led by S. Maruyama.

Conflicts of Interest: The authors declare no conflicts of interest.

Appendix A Compositional Dependence on Closure Temperature

Harrison et al. [26] examined diffusion data for micas in the annite (Fe biotite)–phlogopite (Mg biotite) series and described a strong compositional effect, with an increasing Fe/Mg ratio corresponding to an increase in diffusivity. Grove and Harrison [48] carried out the hydrothermal bulk loss experiments employing radiogenic Ar ($^{40}Ar^*$) to determine whether there is $^{40}Ar^*$ diffusivity in biotite with Fe content. They cast serious doubt upon the view that Ar retentivity in biotite increases simply as a function of Fe content because of the remarkable similarity of the experimental results obtained for Fe–mica biotite and Cooma biotite. Harrison [34] measured radiogenic ^{40}Ar loss from two compositionally contrasting hornblendes with isothermally hydrothermal treatment. The results suggest that the diffusivity of Ar in hornblendes is not sensitive to the Mg/Fe ratio. He also predicts a closure temperature between 578 °C and 490 °C for cooling rates in the range of 500 °C to 5 °C/Ma. Onstott and Peacock [49] examined the argon retentivity of hornblendes from a slowly cooled metamorphic terrane and revealed that the hornblende of the higher Fe/(Fe + Mg + Mn) ratio give the younger Ar/Ar age. They described the closure temperature appears to be correlated with Fe/(Fe + Mg + Mn). Baldwin et al. [50] carried out the isothermally hydrothermal experiments on two compositionally contrasting hornblendes from amphibolite in order to examine the Ar diffusion behavior in metamorphic hornblendes and described that no correlation between the Mg number (Mg/(Mg + Fe) and activation energy was observed.

Thus, these studies suggest that the closure temperatures of the K-Ar biotite and hornblende system seem to depend on the Mg/Fe ratio of minerals. However, the dependence is not significant. Figures A1 and A2 show the variation in the closure temperature (°C) of the biotite and hornblende K-Ar system, for different grain sizes and cooling rates based on the diffusion model by Dodson [33], respectively. These figures show that the influence of grain size and cooling rate is much greater than the compositional dependence mentioned above.

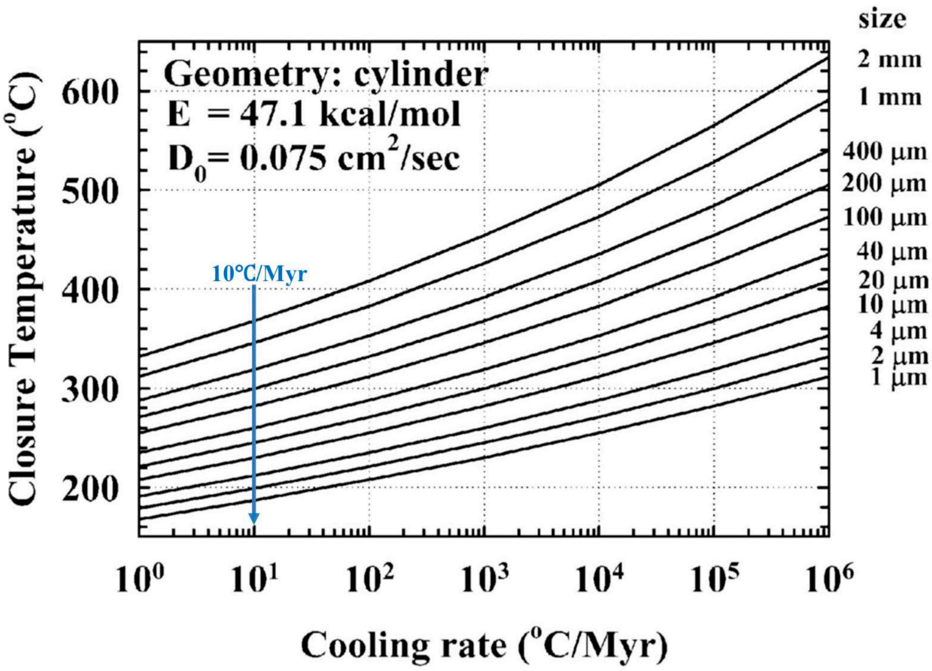

Figure A1. The variation in biotite closure temperature (°C), for different grain sizes and cooling rates based on the diffusion model by Dodson [33] using parameters for biotite by McDougall and Harrison [51]. E and D_0 denote an activation energy and a frequency factor, respectively. The grain size is the diameter of a cylindrical grain. This geometry is appropriate for modeling the diffusion behavior of mica, because of the rapid diffusion perpendicular to the c-axis. This is modified from Figure 5 of Itaya et al. [32].

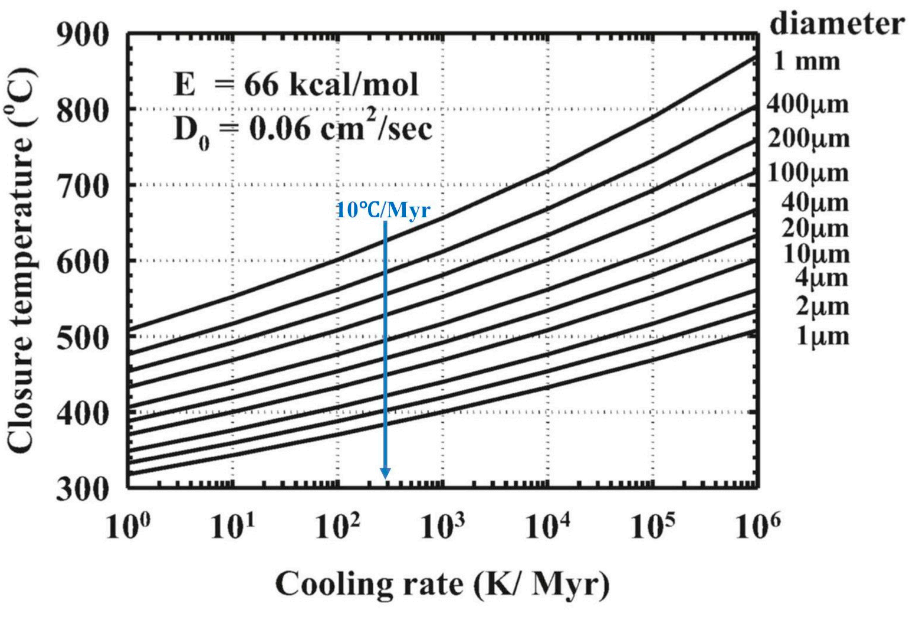

Figure A2. The variation in hornblende closure temperature (°C), for different grain sizes and cooling rates assuming spherical geometry [33]. E and D_0 denote an activation energy and a frequency factor, respectively. This is modified from Figure 1 of Hyodo [52].

Appendix B Excess Argon Wave

The phenomenon of the trapping of excess argon by minerals through argon diffusion was proposed first by Hyodo and York [53]. They found significantly old 'discordant' biotite $^{40}Ar/^{39}Ar$ ages, older than the age of the host lithology, in a narrow zone of a contact aureole and called this phenomenon the 'argon wave (Argonami)' that was renamed the 'Excess–Argon Wave' (EAW) by Itaya et al. [32]. The phenomenon of the trapping of the EAW by minerals has been increasingly observed, also in regional metamorphic sequences. In the Barrovian-type metamorphic complex of the Longmenshan orogen (eastern Tibet), for example, some kyanite-grade metapelites yielded biotite $^{40}Ar/^{39}Ar$ ages 4 to 5 times older than those in the associated sillimanite-grade metapelites [32]; the excess ^{40}Ar was incorporated in biotite by diffusion through the breakdown reaction of muscovite with a significant amount of radiogenic argon. Coexisting biotite and muscovite in the high-grade part of the kyanite zone give ages of 197 Ma and 64 Ma, respectively. This suggests that the trapping of argon by biotite in the excess argon wave took place when the rocks cooled down to temperatures lower than the closure temperature of muscovite but not below that of biotite (Figure A3).

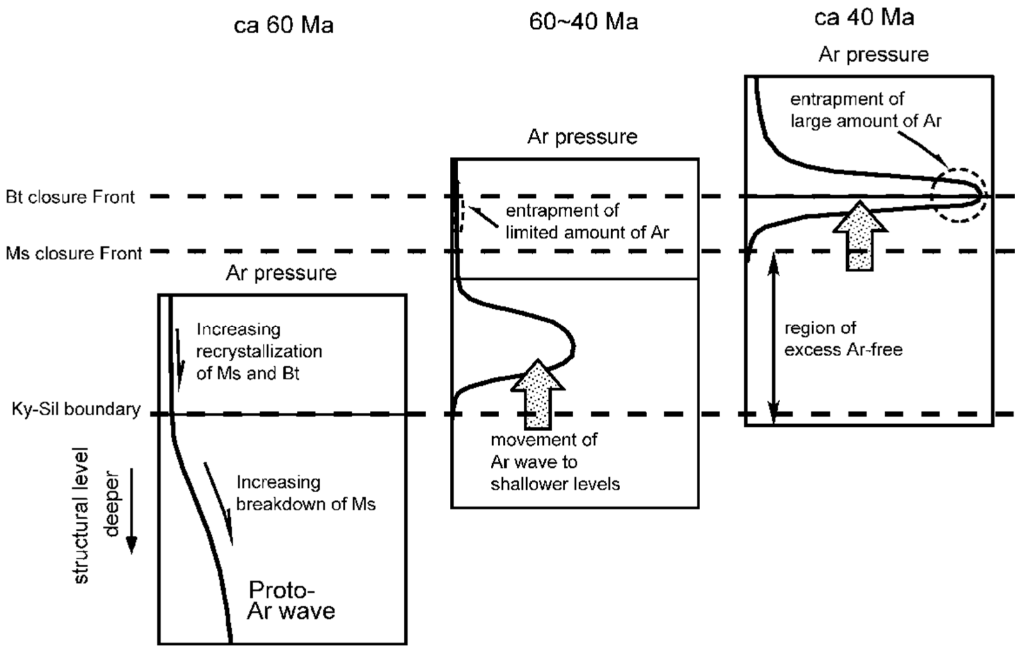

Figure A3. A schematic diagram showing three stages in the development of the envisaged Ar wave and its preservation in biotite, taken from Itaya et al. [32].

Another example is represented by some kyanite grains from the river sand in NE Japan, which gave extremely old $^{40}Ar/^{39}Ar$ ages (8–6 Ga: [54]). These very old ages have been interpreted as due to the fact that kyanite recrystallized in the host rocks under ultra-high argon pressure derived from radiogenic argon in potassium-rich phases such as phengites during the Barrovian-type retrogression of UHP rocks. Similarly, the excess ^{40}Ar-bearing phengite ages obtained for the Gongen eclogite in the Sanbagawa belt, SW Japan, might suggest a phenomenon similar to an EAW [55], because the excess ^{40}Ar was not inherited from precursor older rocks. In this case, it has been demonstrated that the excess ^{40}Ar preserved in the Gongen eclogite formed by the interaction between metagraywacke and metaperidotite with mantle-derived noble gas (a very high $^{40}Ar/^{36}Ar$ ratio of 3500–8000; cf. [56]) at eclogite facies depth. Fluid exchange between deep subducted sediments and mantle material might have enhanced the gain of mantle-derived extreme ^{40}Ar in the metasediments. The high argon pressure environment created by the interaction among metasediments, peridotite, and fluids would have allowed for the trapping of a large amount of excess argon within phengitic micas. Itaya et al. [57] reported excess argon-bearing K-feldspar from metagranite in the UHP Brossasco–Isasca Unit of Dora Maira Massif, Italy, and pointed out the possibility that K-feldspar has trapped the EAW generated by the argon release from micas during the exhumation and cooling of the host lithologies. Itaya et al. [58] carried out laser step-heating $^{40}Ar/^{39}Ar$ analyses of biotite from the same metagranite and found the biotite crystals which have old age fractions (800 to 1300 Ma) three to four times older than that of the granite protolith (which is late Permian). They argued the possible sources of the EAW are the overlying eclogite facies phengitic micaschists of the Variscan basement and/or the underlying blueschist facies micaschists. Thus, instead of the total or partial resetting of the original age, the phenomenon of the trapping of excess argon by minerals through argon diffusion may be quite common in polymetamorphic MP–HP–UHP metamorphic rocks, depending on the closure temperature of minerals and on the presence of transient argon pressure. In particular, biotites older than the hosting rocks must be related to the EAW generated by the argon release from micas during the exhumation and cooling of the hosting lithologies and/or by the heating of country rocks induced by intrusive rocks.

References

1. Hoffman, P.F. Precambrian geology and tectonic history of North America. In *The Geology of North America: An Overview*; Bally, A.W., Palmer, A.R., Eds.; Geological Society of America, Geology of North America: Boulder, CO, USA, 1989; pp. 447–512.
2. Bowring, S.A.; Grotzinger, J.P. Implications of new chronostratigraphy for tectonic evolution of Wopmay orogen, northwest Canadian Shield. *Am. J. Sci.* **1992**, *292*, 1–20. [CrossRef]
3. Bowring, S.A.; Williams, I.S.; Compston, W. 3.96 Ga gneisses from the Slave province, Northwest Territories, Canada. *Geology* **1989**, *17*, 971–975. [CrossRef]
4. Iizuka, T.; Horie, K.; Komiya, T.; Maruyama, S.; Hirata, T.; Hidaka, H.; Windley, B.F. 4.2 Ga zircon xenocryst in an Acasta gneiss from northwestern Canada: Evidence for early continental crust. *Geology* **2006**, *34*, 245–248. [CrossRef]
5. Iizuka, T.; Komiya, T.; Ueno, Y.; Katayama, I.; Uehara, Y.; Maruyama, S.; Hirata, T.; Johnson, S.P.; Dunkley, D.J. Geology and zircon geochronology of the Acasta Gneiss Complex, northwestern Canada: New constraints on its tectonothermal history. *Precanbrian Res.* **2007**, *153*, 179–208. [CrossRef]
6. Guitreau, M.; Mora, N.; Paquette, J.-L. Crystallization and disturbance histories of single zircon crystals from Hadean-Eoarchean Acasta gneisses examined by LA-ICP-MS U-Pb traverses. *Geochem. Geophys. Geosyst.* **2017**, *19*, 272–291. [CrossRef]
7. Hodges, K.V.; Bowring, S.A.; Coleman, D.S.; Hawkins, D.P.; Davide, K.L. Multi-stage thermal history of the ca. 4.0 Ga Acasta gneisses. *Eos Trans. AGU* **1995**, *76*, F708.
8. Padgham, W.A.; Fyson, W.K. The Slave Province: A distinct Archean craton. *Can. J. Earth Sci.* **1992**, *29*, 2072–2086. [CrossRef]
9. van Breemen, O.; Davis, W.J.; King, J.E. Temporal distribution of granitoid plutonic rocks in the Archean Slave Province, northwest Canadian Shield. *Can. J. Earth Sci.* **1992**, *29*, 2186–2199. [CrossRef]
10. Bowring, S.A.; Housh, T.B.; Isachsen, C.E. *The Acasta Gneisses: Remnant of Earth's Early Crust. Origin of the Earth*; Oxford University Press: New York, NY, USA, 1990.
11. Bowring, S.A.; Williams, I.S. Priscoan (4.00–4.03 Ga) orthogneisses from northwestern Canada. *Contrib. Miner. Petrol.* **1999**, *134*, 3–16. [CrossRef]
12. Reimink, J.R.; Davies, J.H.F.L.; Chacko, T.; Stern, R.; Heaman, L.; Sarkar, C.; Schaltegger, U.; Creaser, R.A.; Pearson, D.G. No evidence for Hadean continental crust within Earth's oldest evolved rock unit. *Nat. Geosci.* **2016**, *9*, 777–780. [CrossRef]
13. Reimink, J.R.; Chacko, T.; Chacko, T.; Carlson, R.W.; Shirey, S.B.; Liu, J.; Stern, R.A.; Bauer, A.M.; Pearson, D.G.; Heaman, L.M. Petrogenesis and tectonics of the Acasta Gneiss Complex derived from integrated petrology and ^{142}Nd and ^{182}W extinct nuclide-geochemistry. *Earth Planet Sci. Lett.* **2018**, *494*, 12–22. [CrossRef]
14. Reimink, J.; Pearson, D.; Shirey, S.; Carlson, R.; Ketchum, J. Onset of new, progressive crustal growth in the central Slave craton at 3.55 Ga. *Geochem. Perspect. Lett.* **2019**, *10*, 8–13. [CrossRef]
15. Reimink, J.R.; Davies, J.H.; Bauer, A.M.; Chacko, T. A comparison between zircons from the Acasta Gneiss Complex and the Jack Hills region. *Earth Planet. Sci. Lett.* **2020**, *531*, 115975. [CrossRef]
16. Hoffman, P.F.; Tirrul, R.; King, J.E.; St-Onge, M.R.; Lucas, S.B. Axial projections and modes of crustal thickening, eastern Wopmay orogen, northwest Canadian Shield. In *Processes in Continental Lithospheric Deformation*; Clark, S.P., Jr., Ed.; Geological Society of America: Boulder, CO, USA, 1988; Volume 218, pp. 1–29.
17. Hildebrand, R.S.; Hoffman, P.F.; Bowring, S.A. The Calderian orogeny in Wopmay orogen (1.9 Ga), northwestern Canadian Shield. *GSA Bull.* **2010**, *122*, 794–814. [CrossRef]
18. Hoffman, P.F. Evolution of an early Proterozoic continental margin: The Coronation geosyncline and associated aulacogens of the northwestern Canadian Shield. *R. Soc. Lond. Philos. Trans.* **1973**, *273*, 547–581.
19. Hoffman, P.F.; St-Onge, M.R.; Easton, R.M.; Grotzinger, J.; Schulze, D.L. Syntectonic plutonism in north-central Wopmay orogen (early Proterozoic), Hepburn Lake map area, District of Mackenzie. *Curr. Res. Part A Geol. Surv. Can. Pap.* **1980**, *80*, 171–177.
20. Housh, T.; Bowring, S.A.; Villeneuve, M. Lead isotopic study of early Proterozoic Wopmay orogen, NW Canada: Role of continental crust in arc magmatism. *J. Geol.* **1989**, *97*, 735–747. [CrossRef]
21. Bowring, S.A.; Podosek, F.A. Nd isotopic evidence from Wopmay orogen for 2.0–2.4 Ga crust in western North America. *Earth Planet. Sci. Lett.* **1989**, *94*, 217–230. [CrossRef]

22. Hildebrand, R.S.; Bowring, S.A.; Housh, T. The Medial zone of Wopmay orogen, District of Mackenzie. *Curr. Res. Part C Geol. Surv. Can. Pap.* **1990**, *90*, 167–176.
23. Nagao, K.; Nishido, H.; Itaya, T.; Ogata, K. K–Ar age determination method. *Bull. Hiruzen Res. Inst.* **1984**, *9*, 19–38.
24. Itaya, T.; Nagao, K.; Inoue, K.; Honjou, Y.; Okada, T.; Ogata, A. Ar isotope analysis by a newly developed mass spectrometric system for K–Ar dating. *Mineral. J.* **1991**, *15*, 203–221. [CrossRef]
25. Steiger, R.H.; Jäger, E. Subcommission on geochronology: Convention on the use of decay constants in geo– and cosmochronology. *Earth Planet. Sci. Lett.* **1977**, *36*, 359–362. [CrossRef]
26. Harrison, T.M.; Duncan, I.; McDougall, I. Diffusion ^{40}Ar in biotite: Temperature, pressure and composition. *Geochim. Cosmochim. Acta* **1985**, *49*, 2461–2468. [CrossRef]
27. Hyodo, H.; Kim, S.; Itaya, T.; Matsuda, T. Homogeneity of neutron flux during irradiation for ^{40}Ar/^{39}Ar age dating in the research reactor at Kyoto University. *J. Mineral. Petrol. Sci.* **1999**, *94*, 329–337. [CrossRef]
28. Hyodo, H.; Itaya, T.; Matsuda, T. Temperature measurement of small minerals and its precision using Laser heating. *Bull. Res. Inst. Nat. Sci. Okayama Univ. Sci.* **1995**, *21*, 3–6, (In Japanese with English Abstract).
29. Hyodo, H.; Matsuda, T.; Fukui, S.; Itaya, T. ^{40}Ar/^{39}Ar age determination of a single mineral grain by Laser step heating. *Bull. Res. Inst. Nat. Sci. Okayama Univ. Sci.* **1994**, *20*, 63–67.
30. Roddick, J.C. High precision intercalibration of ^{40}Ar–^{39}Ar standards. *Geochim. Cosmochim. Acta* **1983**, *47*, 887–898. [CrossRef]
31. Itaya, T. K-Ar phengite geochronology of HP-UHP metamorphic rocks-An in-depth review. *J. Mineral. Petrol. Sci.* **2020**, *115*, 44–58. [CrossRef]
32. Itaya, T.; Hyodo, H.; Tsujimori, T.; Wallis, S.; Aoya, M.; Kawakami, T.; Gouzu, C. Regional-Scale Excess Ar wave in a Barrovian type metamorphic belt, eastern Tibetan Plateau. *Isl. Arc.* **2009**, *18*, 293–305. [CrossRef]
33. Dodson, M.H. Closure temperature in cooling geochronological and petrological systems. *Contrib. Mineral. Petrol.* **1973**, *40*, 259–274. [CrossRef]
34. Harrison, T.M. Diffusion of ^{40}Ar amphibole. *Contrib. Mineral. Petrol.* **1981**, *78*, 324–331. [CrossRef]
35. Sano, Y.; Terada, K.; Hidaka, H.; Yokoyama, K.; Nutman, A.P. Palaeoproterozoic thermal events recorded in the ~4.0 Ga Acasta gneiss, Canada: Evidence from SHRIMP U-Pb dating of apatite and zircon. *Geochim. Cosmochim. Acta* **1999**, *63*, 899–905. [CrossRef]
36. St-Onge, M.R. Zoned poikiloblastic garnets: Documentation of P-T paths and syn-metamorphic uplift through thirty kilometers of structural depth, Wopmay orogen, Canada. *J. Petrol.* **1987**, *28*, 1–21. [CrossRef]
37. St-Onge, M.R. Geothermometry and geobarometry in pelitic rocks of north-central Wopmay orogen (early ProterozoicNorthwest Territories, Canada. *Geol. Soc. Am. Bull.* **1984**, *95*, 196–208. [CrossRef]
38. Lalonde, A.E. Hepburn intrusive suite: Peraluminous plutonism within a closing back-arc basin, Wopmay orogen, Canada. *Geology* **1989**, *17*, 261–264. [CrossRef]
39. Ishihara, S. The magnetite-series and ilmenite-series granitic rocks. *Min. Geol.* **1977**, *27*, 293–305.
40. Isozaki, Y.; Aoki, K.; Nakama, T.; Yanai, S. New insight into a subduction-related orogen: Reappraisal on geotectonic framework and evolution of the Japanese Islands. *Gondwana Res.* **2010**, *18*, 82–105. [CrossRef]
41. Nakajima, T.; Takahashi, M.; Imaoka, T.; Shimura, T. Granitic rocks. In *The Geology of Japan*; Moreno, T., Wallis, S., Kojima, T., Gibbons., W., Eds.; Geological Society: London, UK, 2016; pp. 251–272.
42. Ikeda, T. Pressure-Temperature conditions of the Ryoke metamorphic rocks in the Yanai district, SW Japan. *Contrib. Mineral. Petrol.* **2004**, *146*, 577–589. [CrossRef]
43. D'Lemons, R.S.; Brown, M.; Strachan, R.A. Granite magma generation, ascent and emplacement within a transpressional orogen. *J. Geol. Soc.* **1992**, *149*, 487–490. [CrossRef]
44. Bons, P.D.; Arnold, J.; Elburg, M.A.; Kalda, J.; Soesoo, A.; Milligan, B.P. Melt extraction and accumulation from partially molten rocks. *Lithos* **2004**, *78*, 25–42. [CrossRef]
45. Ohira, T. Cretaceous Fore Arc Volcanism in SW Japan. Master's Thesis, Okayama University of Science, Okayama, Japan, 1995.
46. Imaoka, T.; Kawaba, H.; Nagashima, M.; Nakashima, K.; Kamei, A.; Yagi, K.; Itaya, T.; Kiji, M. Petrogenesis of an Early Cretaceous lamprophyre dike from Kyoto Prefecture, Japan: Implications for the generation of high-Nb basalt magmas in subduction zones. *Lithos* **2017**, *290–291*, 18–33. [CrossRef]
47. Fukui, S.; Tsujimori, T.; Watanabe, T.; Itaya, T. Tectono-metamorphic evolution of high-P/T and low-P/T metamorphic rocks in the Tia Complex, southern New England Fold Belt, eastern Australia: Insights from K–Ar chronology. *J. Asian Earth Sci.* **2012**, *59*, 62–69. [CrossRef]
48. Grove, M.; Harrison, T.M. ^{40}Ar* diffusion in Fe-rich biotite. *Am. Mineral.* **1966**, *81*, 940–951. [CrossRef]
49. Onstott, T.C.; Peacock, M.W. Argon retentivity of hornbledes: A field experiment in slowly cooled metamorphic terrane. *Geochim. Cosmochim. Acta* **1987**, *51*, 2891–2903. [CrossRef]
50. Baldwin, S.L.; Harrison, T.M.; Gerald, J.D.F. Diffusion of ^{40}Ar in metamorphic hornblende. *Contrib. Mineral. Petrol.* **1990**, *105*, 691–703. [CrossRef]
51. McDougall, I.; Harisson, T.M. *Geochronology and Thermochronology by the ^{40}Ar/^{39}Ar Method*, 2nd ed.; Oxford University Press: Oxford, UK, 1999.
52. Hyodo, H. Closure temperature estimate of hornblende using laser heating results. *Bull. Res. Inst. Nat. Sci.* **2014**, *40*, 53–58, (In Japanese with English Abstract).

53. Hyodo, H.; York, D. The discovery and significance of a fossilized radiogenic argon wave (argonami) in the earth's crust. *Geophys. Res. Lett.* **1993**, *20*, 61–64. [CrossRef]
54. Itaya, T.; Hyodo, H.; Uruno, K.; Mikoshiba, M.-U. Ultra–high excess argon in kyanites: Implications for ultra–high pressure metamorphism in Northern Japan. *Gondwana Res.* **2005**, *8*, 617–621. [CrossRef]
55. Itaya, T.; Tsujimori, T. White mica K–Ar geochronology of the Sanbagawa eclogites in SW Japan: Implications on deformation–controlled K–Ar closure temperature. *Int. Geol. Rev.* **2015**, *57*, 1014–1022. [CrossRef]
56. Kaneoka, I.; Takaoka, N. Rare gas isotopes in Hawaiian ultramafic nodules and volcanic rocks: Constraint on genetic relationships. *Science* **1980**, *208*, 1366–1368. [CrossRef]
57. Itaya, T.; Yagi, K.; Gouzu, C.; Thanh, N.X.; Groppo, C. Preliminary report on the excess argon bearing Orthoclase from metagranite in the Brossasco–Isasca UHP Unit of Dora–Maira Massif, Italy. *J. Mineral. Petrol. Sci.* **2017**, *112*, 36–39. [CrossRef]
58. Itaya, T.; Hyodo, H.; Imayama, T.; Groppo, C. Laser step-heating $^{40}Ar/^{39}Ar$ analyses of biotites from meta-granites in the UHP Brossasco-Isasca Unit of Dora-Maira, Italy. *J. Mineral. Petrol. Sci.* **2018**, *113*, 171–180. [CrossRef]